Received/Accepted
Preprint typeset using LaTeX style emulateapj v. 10/09/06

SPECTACULAR TRAILING STREAMERS NEAR LMC X-1: THE FIRST EVIDENCE OF A JET?

Ryan Cooke[1], Zdenka Kuncic[1], Rob Sharp[2] & Joss Bland-Hawthorn[2]

Received/Accepted

ABSTRACT

We report VIMOS integral field spectroscopy of the N159F nebula surrounding LMC X-1. Our observations reveal a rich, extended system of emission line filaments lining the boundary of a large conical cavity identified in *Spitzer* mid-IR imaging. We find that X-ray photoionization cannot be solely responsible for the observed ionization structure of N159F. We propose that the extended filamentary emission is produced primarily by ionization from a shock driven by a presently unobserved jet from LMC X-1. We infer a shock velocity of $v_s \approx 90\,\mathrm{km\,s^{-1}}$ and conclude that the jet responsible for the bow shock is presently undetected because it has switched off, rather than because it has a low surface brightness. This interpretation is consistent with the present soft X-ray spectral state of LMC X-1 and suggests the jet is intermittent.

Subject headings: accretion — ISM: jets and outflows — techniques: spectroscopic — X-rays: binaries — X-rays: individual (LMC X-1)

1. INTRODUCTION

LMC X-1 resides in the highly complex nebula region N159 (Henize 1956). It is the most powerful known X-ray source in the LMC (Johnston, Bradt & Doxsey 1979), with an X-ray luminosity $L_X \approx 2 \times 10^{38}\mathrm{erg\,s^{-1}}$ (Schlegel et al. 1994), and is believed to be powered by accretion onto a stellar mass $(4 - 10\,M_\odot)$ black hole with a companion O7 III-type star identified as star 32 (Pakull & Angebault 1986; Cowley 1992). Pakull & Angebault (1986) collated extensive spectral data and ruled out collisional excitation by a supernova remnant. They concluded that their detection of He II emission is the first evidence for an X-ray ionized nebula (see also Ramsey et al. 2006). We note, however, that the slit spectra used in these studies were limited to a relatively localized region of the nebula, in the immediate vicinity of LMC X-1.

Using integral field spectroscopy (IFS), we present new evidence suggesting that X-ray photoionization cannot be solely responsible for the observed large scale morphology and high excitation lines, which we propose are best understood in terms of shock ionization attributable to an as yet undetected relativistic jet from LMC X-1. Indeed, the highly complex ionization structure of the extended nebula surrounding LMC X-1 is strikingly reminiscent of the other two only known examples of jet-induced shock ionized nebulae, those surrounding the powerful Galactic X-ray binaries SS433 (Dubner et al. 1998) and Cygnus X-1 (Gallo et al. 2005).

We were initially alerted to the possibility of shock ionization in N159F after observing with the Taurus Tunable Filter (TTF) at the Anglo-Australian Telescope (Bland-Hawthorn & Jones 1998) in 2003 December. We discovered a rich system of streaming Hα filaments in the arcmin-scale nebula. The filaments trail back from the apex of a conical cavity in the dust emission seen in the *Spitzer* Infrared Array Camera (IRAC) image of Jones et al. (2005). The apex is positioned $\approx 12''$ South-West of LMC X-1, corresponding to $\approx 3.2\,\mathrm{pc}$ at a distance $d \approx 55\,\mathrm{kpc}$ to the LMC (Feast 1999).

Motivated by these observations, we undertook further investigation into the environment of LMC X-1 through integral field spectroscopy (IFS) with VIMOS at the Very Large Telescope (VLT) in 2005 November. The new data reveal strong detections of optical emission lines due to [O I], [N II], [S II], He I and [Ar III], as well as Hα. The emission lines all show a similar morphological bow shock structure as the initial Hα filamentary streamers seen in the TTF image. In Figure 3 of Jones et al. (2005), which overlays the 5 GHz radio contours of Hunt & Whiteoak (1994) on an IR image of N159, radio emission appears to trace the IRAC cavity.

We summarize the observations and data reduction procedures in § 2. In § 3, we present our results and provide an interpretation of the environment of LMC X-1. Our conclusions are summarized in § 4.

2. OBSERVATIONS AND DATA ANALYSIS

Our initial TTF observations of the N159F nebula were taken in a 5 Å bandpass centred on Hα. A powerful differential technique called 'straddle shuffling' (Maloney & Bland-Hawthorn 2001) was used to remove the surrounding continuum emission to better than 1% accuracy, revealing the filamentary structure of the nebula. These data prompted observations with the VIMOS integral field unit (IFU) at the VLT on 2005 November 2, 5, 6. Conditions were reported as photometric, with $1.4'' - 1.5''$ seeing (well matched to the $0.67''$ spatial scale of the IFU). Observations were queue scheduled using the HR-Orange grating (R $\approx$ 2500, $\lambda\lambda$5250-7400Å) and include the emission lines Hα, [O I], [N II], [S II], He I, and [Ar III]. The systemic radial velocity ($v_r \approx 270\,\mathrm{km\,s^{-1}}$) of the LMC ensures that the [O I] and Hα emission lines are well separated from their telluric counterparts.

Given the $27'' \times 27''$ field-of-view of the VIMOS IFU in high resolution mode, four VIMOS pointings were required (with a 5 pixel/$3.3''$ overlap) to tile the Hα

Electronic address: r.cooke@physics.usyd.edu.au
[1] School of Physics, University of Sydney, NSW, Australia
[2] Anglo-Australian Observatory, Epping, NSW, Australia

filaments along the boundaries of the Mid-IR cavity in the vicinity of LMC X-1. Three 1160 sec exposures were taken at each of the four pointings. The data were reduced using the reduction pipeline VIPGI[3] (see Scodeggio et al. 2005, for details). Datacubes were created and sub-sections of the final mosaic were combined using a set of IFU data manipulation routines created in IDL. Emission line fitting was performed for each prominent spectral line using a single unresolved Gaussian profile.

Due to the restricted spectral coverage of the chosen VIMOS setting, the key shock diagnostic line [O III]λ5007 is not present in our data. However, we retrieved archival [O III] observations from the public ESO archive. The 2.3 m WFI observations[4] of N159F consists of 2×500 sec observations using the [O III] filter and 2×125 sec observations using the R_c filter. The data were processed in the usual manner (overscan corrected, flat-fielded from twilight flat frames, aligned and combined) using elements of the CASU imaging processing toolkit (Irwin & Lewis 2001). Continuum subtraction was achieved for the [O III] and Hα narrow band images using the aligned and scaled V and R_c images respectively. The WFI and VIMOS data were spatially registered and resampled using stellar images common to both data sets.

3. RESULTS & DISCUSSION

Figure 1 shows the main results from the new VIMOS, WFI and IRAC observations. Together, these provide compelling evidence for shock ionization in the N159F nebula surrounding LMC X-1. Fig. 1(a-d) show, respectively, the prominent emission lines Hα, [Ar III] and [O I] in the VIMOS data cube, and [O III] from the continuum subtracted WFI data. A bow shock morphology, with trailing filaments, is evident in the images. Fig. 1(e) shows a line diagnostics plot formed from a pixel-pixel comparison of [O III]/[O I] vs. [Ar III]/[S II] where four color-coded ionization regions show spatial coherence over the N159F nebula (see Fig. 1(f)). Fig. 1(h) is a 3-color *Spitzer* IRAC image centered on star 32 (Jones et al. 2005), showing a dust cavity associated with the proposed bow shock. Fig. 1(k) presents a 3-color composite image in [N II] (red), Hα (green) and [O I] (blue). We speculate that the shock is driven by a jet, with orientation indicated in Fig. 1(k).

3.1. *Disentangling the Shock-Ionized Nebula*

Separating out the shock-ionized part of the optical nebula is not straightforward, as radiative shocks can produce collisionally excited optical emission lines similar to those produced by X-ray photoionization (see e.g. Dopita & Sutherland 2003). Both ionization mechanisms can produce enhanced (relative to H II regions) Hα as well as enhanced forbidden lines of neutral or low ionization species, such as [O I]λ6300, [S II]$\lambda\lambda$6716,6731 and [N II]$\lambda\lambda$6548,6583, and of higher ionization species, such as [O III]$\lambda\lambda$5007,4959 and [Ar III]λ7136. He II λ4686 is a reliable X-ray photoionization diagnostic as it is difficult to produce with shock ionization, while [Ar III] is difficult to produce with X-ray photoionization, except for very high ionization parameters (R. Sutherland, private communication). Furthermore, X-ray photoionization tends to favour the production of [O III] over [O I] (Draine & McKee 1993). On the other hand, [O III] can be a powerful shock diagnostic, since all radiative shock models (Cox & Raymond 1985; Binette, Dopita & Tuohy 1985; Hartigan, Raymond & Hartmann 1987) consistently predict a dramatic onset of [O III] emission near a critical shock speed, $v_s \simeq 100\,\mathrm{km\,s^{-1}}$.

Whilst the Hα and [Ar III] images in Fig. 1(a) and (b) exhibit a similar morphological structure suggestive of a bow shock, a comparison of the [O I] and [O III] images in Fig. 1(c) and (d) shows regions of anticorrelation in the immediate vicinity of LMC X-1 and around the B5 I star R148 (Feast, Thackeray & Wesserlink 1960), where there is a deficit of [O I] emission, but enhanced [O III] emission. R148 is not capable of producing this high excitation emission. Indeed, its Strömgren sphere ($r_s \approx 0.04$ pc) does not even encompass one pixel of our image. The Strömgren radius for star 32 (the O7 III companion to LMC X-1 – Cui et al. 2002) is ≈ 0.9 pc, comparable to the size of the blue region defined in Fig. 1(e) and (f). Recalling that X-ray photoionization favours [O III] over [O I] and can produce [Ar III] for high ionization parameters, this blue region, which exhibits the largest local enhancement in [O III]/[O I] and [Ar III]/[S II], must be due to the combined effects of X-ray ionization by LMC X-1 and photoionization by star 32. The yellow region in Fig. 1(e) and (f) is consistent with the extent of the X-ray Strömgren radius ($\simeq 2$ pc), calculated by Pakull & Angebault (1986). Note, however, that this yellow region is located to the East (left) of R148, on the far side of LMC X-1 and spatially coincides with some of the streamers. Thus, we interpret the yellow zone of enhanced [Ar III]/[S II] and [O III]/[O I] as being due to a combination of shock ionization and X-ray ionization. The red zone in Fig. 1(e) and (f) is predominantly shock-ionized. Fig. 1(i) and (j) show a proposed trail of streamers through this shock-ionized region.

The evidence for X-ray photoionization in N159F has hitherto been based on slit spectra of He II λ4686 emission detected in the immediate vicinity of LMC X-1 (Pakull & Angebault 1986; Ramsey et al. 2006). In Fig. 1(l), we show the positioning of the echelle slits used by Ramsey et al. (2006) to detect the He II emission. Pakull & Angebault (1986) used similarly placed orthogonal slits, but centred on star 32 instead of R148. Note that although the echelle slits coincide with the yellow zone we identify as being both shock ionized and X-ray ionized, the observed He II λ4686 emission is almost certainly due to only X-ray ionization as none of the radiative shock models predict significant He II λ4686. Note also that it would have been extremely difficult to find unequivocal evidence for shock ionization from other line diagnostics due to the confusion with X-ray ionization in this region and also to the spatially limited extent of the slits. On scales of several parsecs, our IFU data reveal enhanced [O I]/Hα, [O III], and [Ar III], as well as Hα, forming a shell-like structure around LMC X-1, but extending beyond the X-ray Strömgren radius (that is, beyond the yellow zone in Fig. 1(e) and (f)). This is compelling evidence that shock-ionization rather than X-ray ionization

[3] VIPGI - Vimos Interactive Pipeline Graphical Interface, obtained from *http://cosmos.iasf-milano.inaf.it/pandora/*

[4] Program ID: 076.D-0017(A)

is primarily responsible for this high-excitation emission seen on the largest scales in the nebula.

3.2. *Physical parameters*

Fig. 1(g) shows an image of the electron number density, N_e, deduced from the [S II] emission (Osterbrock & Ferland 2006). It reveals an enhanced flattened region that falls slightly inside and near the apex of the bow-shock morphology. This structure is highly suggestive of a 'Mach disk' commonly seen in bow shocks associated with Herbig-Haro jets (Hartigan et al. 1999). In the flattened region, we find $N_e \approx 1600\,\mathrm{cm}^{-3}$, a factor $\approx$3 times greater than the environment. This is less than the maximum compression ratio of 4 expected for a strong shock, but is compatible with the Mach number inferred from the shock speed (see below).

From the high density region, we can determine a shock speed using the multitude of line ratios extracted from a single IFS exposure. Fig. 1(m) shows theoretical line ratios from the radiative shock model of Hartigan et al. (1987). The dashed horizontal lines indicate the maximum and minimum shock speeds obtained from the new data for each corresponding line ratio. From the presence of [O III], we infer a lower limit $v_s \gtrsim 80\ \mathrm{km\,s^{-1}}$. [Ar III]/He I suggests $v_s \lesssim 190\,\mathrm{km\,s^{-1}}$, while both the [S II]/Hα and [Ar III]/Hα line ratios further constrain the shock velocity to $v_s \approx 90 - 100\,\mathrm{km\,s^{-1}}$. Thus, we estimate a shock speed $v_s \approx 90\,\mathrm{km\,s^{-1}}$, as indicated by the black dashed vertical line in Fig. 1(m). This is broadly consistent with the line profiles being marginally resolved at $\approx 120 - 150$ km s^{-1} FWHM within the high density region. It also implies a Mach number of ≈ 6, assuming an isothermal sound speed $\approx 14\,\mathrm{km\,s^{-1}}$ for an ambient gas temperature of 10^4 K. We note, however, that the deduced value of v_s is likely to be somewhat overestimated, as the Hartigan et al. (1987) shock model assumes a neutral pre-shock medium, and this produces a spectrum similar to preionized, shocked material with a lower v_s (Cox & Raymond 1985).

3.3. *Energy Budget*

The streamers are unlike the uniform wind-blown bow shocks associated with OB-runaway stars (see e.g. Kaper et al. 1997). Indeed, the the inferred space velocity $v_\star$ of the O7 III companion is too low to be consistent with this interpretation. We estimate $v_\star \sim 0.4\,(\dot{M}_w/10^{-7}\,M_\odot\,\mathrm{yr}^{-1})^{1/2}\,v_{w,1500}^{1/2}\,(\rho_a/6 \times 10^{-22}\,\mathrm{g\,cm^{-3}})^{-1/2}\,R_{3.2}^{-1}\,\mathrm{km\,s^{-1}}$ (Kaper et al. 1997), where $v_w = 1500\,v_{w,1500}$ and $\dot{M}_w$ are the wind velocity and mass loss rates of star 32 (Pakull & Angebault 1986), ρ_a is the mass density of the ambient medium, deduced from the [S II] lines (§ 3.2), using an ionization fraction of $x \approx 1$, and where $R = 3.2\,R_{3.2}$ is the distance between star 32 and the stagnation point (apex), which has an angular distance 12″ corresponding to $\gtrsim 3.2$ pc, where the inequality takes into account projection effects. We henceforth consider the possibility that the shock is produced by a jet from LMC X-1.

Adopting the "dentist drill" model of Scheuer (1974), a cavity, or cocoon, develops naturally around a jet ploughing through the ambient ISM. A shock develops around the cocoon and the shocked gas then comes into dynamical (ram) pressure equilibrium with the jet. Thus, $\rho_j v_j^2 \approx \rho_s v_s^2$, where ρ_j and ρ_s are the mass densities of the jet and shocked gas, respectively, and v_j and v_s are the corresponding speeds. The total jet kinetic power is $P_j \approx \pi(\phi_j z_j)^2 \rho_j v_j^3$ (assuming it is not too relativistic), where ϕ_j is the jet half opening angle and z_j is the jet length (distance to the impact site, at the apex of the cocoon, from LMC X-1). Thus, $P_j \simeq 2 \times 10^{39}\,v_{j,0.1}\,(\phi_{j,10}\,z_{j,3.2}\,v_{s,90})^2\,(\rho_s/2 \times 10^{-21}\,\mathrm{g\,cm^{-3}})\,\mathrm{erg\,s^{-1}}$. Here, $\phi_{j,10} = \phi_j/10°$ (Miller-Jones, Fender & Nakar 2006 find an upper limit of $\phi_j \lesssim 10°$ for X-ray binary jets), $z_{j,3.2} = z_j \sin^{-1}\theta/(3.2\,\mathrm{pc})$ and θ is the jet inclination angle to our line-of-sight. We have used a post-shock electron number density $N_e \approx 1.6 \times 10^3\,\mathrm{cm^{-3}}$ (§ 3.2) to estimate ρ_s. This estimate of jet power falls squarely within the range $P_j \approx 10^{37-42}\,\mathrm{erg\,s^{-1}}$ estimated by Fender & Pooley (2000) for quasi-steady X-ray binary jets.

It is noteworthy, however, that LMC X-1 currently appears to be in a persistent high/soft X-ray spectral state (Schlegel et al. 1994), during which it is unlikely to be producing a powerful jet (Fender, Belloni & Gallo 2004) and its X-ray luminosity is dominated by the accretion disk, which radiates away all the accretion power. Since the accretion power inferred from the observed X-ray luminosity, $\approx 2 \times 10^{38}\,\mathrm{erg\,s^{-1}}$, is an order of magnitude less than the inferred jet power, we suggest that rather than being a dark jet (as Gallo et al. 2005 proposed for Cyg X-1, which is in a low/hard spectral state), the non-detection of the LMC X-1 jet results from the inherent transient nature of X-ray binary jets. The jet is not presently seen because it may have recently switched off and the shock-ionized nebula surrounding LMC X-1 is still radiating the energy impacted during an earlier jet-active epoch. We estimate a radiative cooling timescale of just $\sim 10^2$ yrs, assuming 0.3 solar metallicity (Dopita & Sutherland 2003). The jet-active phase may have been triggered by a relatively sudden increase in the mass accretion rate, which has a present value $\dot{M}_a \approx 12 L_X/c^2 \approx 4 \times 10^{-8}\,M_\odot\,\mathrm{yr}^{-1}$ (assuming a radiative efficiency of $\frac{1}{12}$ for standard thin disk accretion). The dynamical timescale over which the jet-driven shock has been expanding into the ISM is estimated as $t_{dyn} \sim z_j/v_s \gtrsim 0.03$ Myr, which is remarkably similar to jet lifetime estimates obtained for other X-ray binaries (Gallo et al. 2005; Kaiser et al. 2004).

4. CONCLUSIONS

We have demonstrated the extraordinary power of integral field spectroscopy in our study of the emission-line nebula N159F around LMC X-1. Different emission-line diagnostics have been combined to separate out different ionization regions on extended scales. We propose that three ionizing sources contribute to the complex nature of N159F: 1. photoionization by star 32 (the O7 III companion to LMC X-1); 2. X-ray photoionization by LMC X-1 itself; and 3. jet-driven shock ionization. The first two phenomena are relatively localized, whereas shock ionization dominates over the extended streamers, which appear to be bounded by a bow-shock morphology The morphology and ionization properties of the extended nebula around LMC X-1 are strikingly similar to those seen in other known jet-driven shock ionized

nebulae around Galactic X-ray binaries. We infer a shock speed of $v_s \approx 90$ km s^{-1} and deduce the power of the jet driving the shock to be $\approx 2\times10^{39}$ erg s^{-1}. Since LMC X-1 is unlikely to be producing a jet in its current X-ray spectral state, we propose that the jet is intermittent, with a characteristic lifetime of ~ 0.03 Myr.

We thank an anonymous referee whose comments and suggestions improved the paper considerably. We also thank R. Sutherland, M. Dopita, B. Gaenslar, K. Blundell, and R. Soria for valuable discussions.

REFERENCES

Binette, L., Dopita, M. A., & Tuohy, I. R. 1985, ApJ, 297, 476
Bland-Hawthorn, J. & Jones, D. H. 1998, PASA, 15, 44
Cowley, A. P. 1992, ARA&A, 30, 287
Cox, D. P., & Raymond, J. C. 1985, ApJ, 298, 651
Cui, W., et al. 2002, ApJ, 576, 357
Dopita, M. A., & Sutherland, R. S. 2003, Astrophysics of the Diffuse Universe (Berlin:Springer)
Draine, B. T., & McKee, C. F. 1993, ARA&A, 31, 373
Dubner, G. M., et al. 1998, AJ, 116, 1842
Feast, M. W., Thackeray, A. D., & Wesserlink, A. J. 1960, MNRAS, 121, 337
Feast, M. 1999, in IAU Symp. 190, New Views of the Magellanic Clouds, ed. Y.-H. Chu et al. (San Francisco:ASP), 542
Fender, R. P. & Pooley, G. G. 2000, MNRAS, 318, L1
Fender, R. P., Belloni, T. M. & Gallo, E. 2004, MNRAS, 355, 1105
Gallo, E., et al. 2005, Nature, 436, 819
Hartigan, P., Raymond J., & Hartmann, L. 1987, ApJ, 316, 323
Hartigan, P., Morse, J.A., Tumlinson, J., Raymond, J. & Heathcote, S., 1999, ApJ, 512, 901
Henize, K. G., 1956, ApJS, 2, 315
Hunt, M. R., & Whiteoak, J. B., 1994, PASA, 11, 68
Irwin, M., & Lewis, I. 2001, New A Rev., 45, 105
Johnston, M. D., Bradt, H. V., & Doxsey, R. E. 1979, ApJ, 233, 514
Jones, T. J., et al. 2005, ApJ, 620, 731
Kaiser, C. R., Gunn, K. F., Brocksopp, C. & Sokoloski, J. L. 2004, ApJ, 612, 332
Kaper, L. et al. 1997, ApJ, 475, L37
Maloney, P. R., & Bland-Hawthorn, J. 2001, ApJ, 533, 129
Miller-Jones, J. C. A., Fender, R. P. & Nakar, E. 2006, MNRAS, 367, 1432
Osterbrock, D. E., & Ferland, G. J. 2006, Astrophysics of Gaseous Nebulae and Active Galactic Nuclei (2d ed.; California:University Science Books)
Pakull, M. W., & Angebault, L. P. 1986, Nature, 322, 511
Ramsey, C. J. et al. 2006, ApJ, 641, 241
Scheuer, P. A. G. 1974, MNRAS, 166, 513
Schlegel, E. M., et al. 1994, ApJ, 422, 243
Scodeggio, M., et al. 2005, PASP, 117, 1284

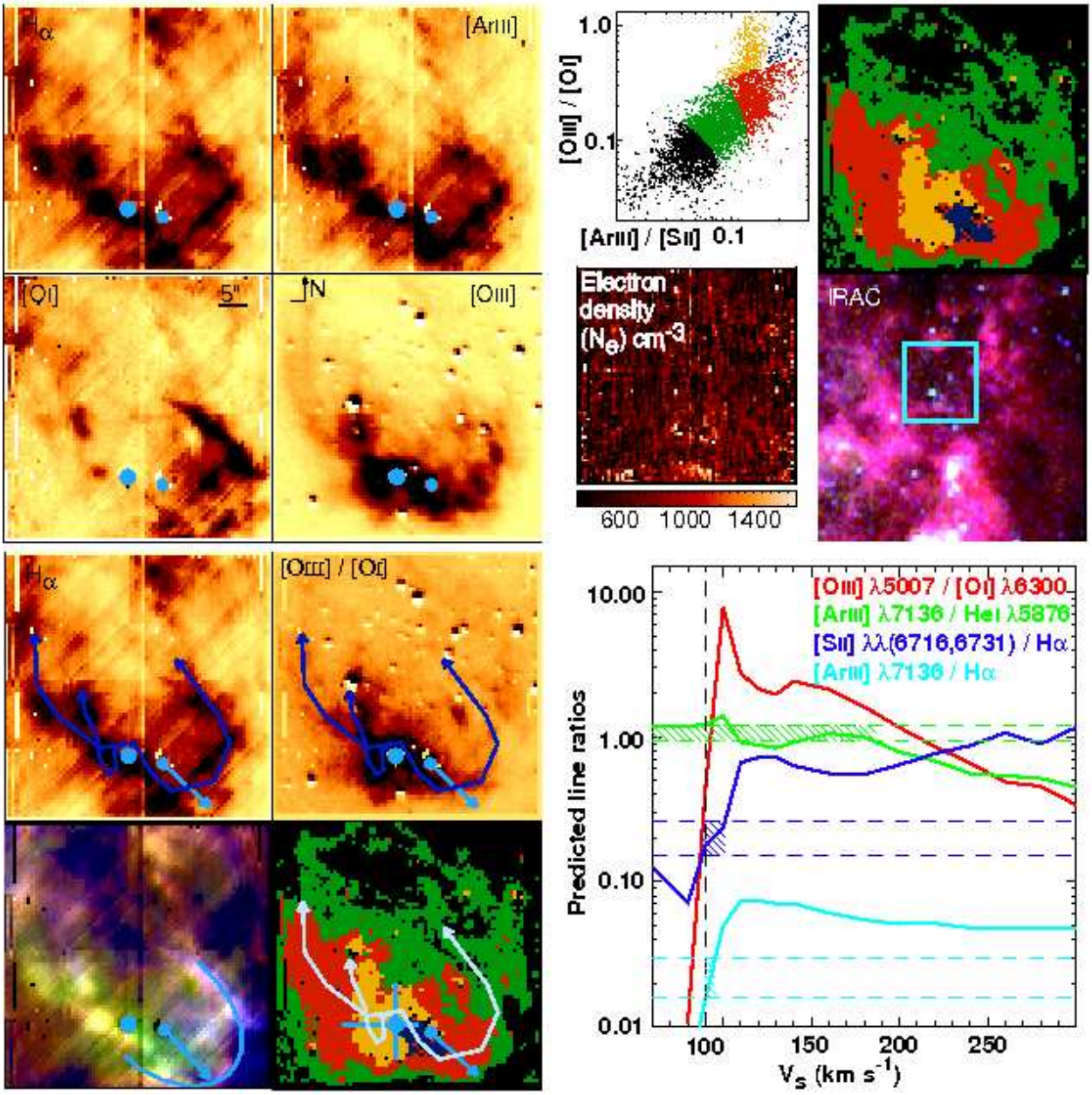

FIG. 1.— (a)–(d) Continuum subtracted integrated line flux images of N159F in Hα, [Ar III], [O I], and [O III]; filled blue circles indicate the locations of stars 32 (right) and R148 (left); north is up and east is to the left ($5'' \approx 1.3$ pc); (e) A diagnostic scatterplot of [O III]λ5007/[O I]λ6300 versus [Ar III]λ7136/[S II]λ(6716+6731); the colour coding corresponds to different ionization regions shown in (f); (g) An electron density image, showing an arc of higher electron density to the south; (h) The *Spitzer* three colour composite image of N159F (Jones et al. 2005), constructed from the IRAC 3.6, 4.5 and 8.0 μm bands; (i)–(j) Hα and [O III]/[O I] images overlaid with a proposed trail of the streamer filaments; (k) A false-colour image (R, G, B = [N II]λ6583, Hα, [O I]λ6300) with the proposed bow shock and jet orientation indicated; (l) Same as (f), with overlaid blue lines indicating the echelle slit positions of Ramsey et al. (2006); grey lines are the proposed streamers; (m) Predicted line ratios and corresponding shock speeds from the radiative shock model in Hartigan et al. (1987) (solid curves) overplotted with observed ranges of line ratios (dashed lines) measured from the region of high electron density shown in (g).